STUDY ON THE SENSITIVITY OF USING MULTIPLE REACTORS AND DETECTORS AT SHORT BASELINES TO OBSERVE STERILE NEUTRINO

Quan-You Chen, Meng Wang

School of Physics
and Key Laboratory of Particle Physics and Particle Irradiation (MOE)
Shandong University, Jinan, 250100, China

(Received April 16, 2015; revised version received July 31, 2015)

In this study, we lay out a proposal of designing a short baseline reactor antineutrino experiment by reusing multiple detectors and commercial reactors in existing resources. A χ^2 function is constructed to evaluate the experimental sensitivity in probing the existence of the sterile neutrino. Several sensitivities for different detector arrangements are studied. It is found that this setup is most sensitive to mass region of the 10^{-2} eV$^2 \lesssim |\Delta m^2_{41}| \lesssim 1$ eV^2 region. For the parameter space with $\Delta m^2_{41} > 1$ eV^2, the sensitivity is limited due to the intrinsic deficiency of the commercial reactor size. In order to probe $\Delta m^2_{41} \sim 1$ eV^2, the distance between the near antineutrino detector (AD) and the near reactor should be less than 30 m and the distance between ADs should be a small value of the order of meters. Sensitivity to $\Delta m^2_{41} \sim$ several $\times\, 0.1$ eV^2 is maximized by a symmetrical detector arrangement relative to the reactors.

DOI:10.5506/APhysPolB.47.1057

1. Introduction

A long series of experiments have demonstrated that neutrinos can mix and oscillate as a result of non-zero neutrino masses [1–9]. In the 3-flavor mixing framework, the three-flavor neutrinos ν_e, ν_μ and ν_τ are unitary linear combinations of three massive neutrinos ν_1, ν_2, ν_3, which have two independent mass squared differences, $\Delta m^2_{21} = m^2_2 - m^2_1 \sim 10^{-5}$ eV^2 and $|\Delta m^2_{31}| = |m^2_3 - m^2_1| \sim 10^{-3}$ eV^2. While the 3-flavor mixing framework successfully describes the data in solar, atmospheric, reactor and accelerator neutrino experiments, a few anomalous results cannot be accommodated in this scheme. The accelerator anomaly, observed in LSND, first attracted attention of the researchers to the idea of the sterile neutrino [10]. The

reactor antineutrino anomaly, observed in recent studies of the impact on the flux of reactor antineutrino, brought forward more hints for the sterile neutrino hypothesis [11–16]. The gallium anomaly, which is observed in the solar neutrino experiments GALLEX and SAGE [17, 18], as well as the dark radiation anomaly that is observed in the cosmological data [19], also provide hints for the existence of the sterile neutrino. If confirmed, it will open a powerful window on our understanding of new physics.

Apart from those hints for sterile neutrino, there are several data sets which do not show any evidence for neutrino oscillation at the eV scale. The results of the global fits to short-baseline (SBL) neutrino oscillation data in the (3+1) framework prefer a mass splitting value of $0.1\ \mathrm{eV}^2 \lesssim |\Delta m^2_{41}| \lesssim 10\ \mathrm{eV}^2$. The best-fit values of Δm^2_{41} in GLO-LOW and GLO-HIG analyses are $0.9\ \mathrm{eV}^2$ and $1.6\ \mathrm{eV}^2$, respectively, in which the GLO-LOW and GLO-HIG are global analyses with and without the three MiniBooNE electron neutrino and antineutrino bins with reconstructed neutrino energy smaller than 475 MeV. Larger values are strongly incompatible with the cosmological constraints on neutrino masses. The result of the global fit assuming one sterile neutrino is bad, thus the (3+1) model may be not sufficient to describe well all data. But considering there are some tensions existing in each scenario, we cannot decide how many additional neutrinos there are at present. We are facing an intriguing accumulation of hints for the existence of sterile neutrino at the eV scale. To confirm or refute the observed anomalies, a number of experiments are running or being designed now [20, 21].

The Daya Bay experiment, which is designed to measure $\sin^2 2\theta_{13}$, has near and far detectors that are located about 500 and 1600 m away from the reactors [22, 23]. There are six reactors and eight movable functionally identical antineutrino detectors (ADs). Its recent results of searching for a light sterile neutrino show that the derived limits on $\sin^2 2\theta_{14}$ cover the $10^{-3}\ \mathrm{eV}^2 \lesssim |\Delta m^2_{41}| \lesssim 0.1\ \mathrm{eV}^2$ region [24]. However, for large Δm^2_{41} values of the order of $1\ \mathrm{eV}^2$, the electron antineutrinos would disappear into sterile neutrino with oscillation lengths of the order of meters. If we want to probe the parameter space with $\Delta m^2_{41} \sim 1\ \mathrm{eV}^2$, the experimental setups should be totally different. In this case, SBL (10–100 m) reactor antineutrino experiments definitely have more advantages. This study aims to investigate the sensitivity of sterile neutrino searches utilizing these ADs transported to a short baseline location near the reactors. The proposed experimental setups have higher probability to probe the favored parameter space in global fits compared to current setups, and can supply more valuable information of the reactor antineutrino spectrum, and extend our understanding of the detectors as well.

2. Method

2.1. Oscillation framework and experimental setups

The additional sterile neutrino states favored in global fits have rather larger mass splittings compared with those active states in 3-flavor mixing framework [20, 21]. As a result, for short baseline experiments, we can write the survival probability in (3+1) model approximately as follows [25]:

$$P_{\text{sur}} \simeq 1 - \sin^2 2\theta_{ee} \sin^2 \left(\frac{1.267 \Delta m^2_{41} L}{E} \right) , \tag{1}$$

where Δm^2_{41} and $\sin^2 2\theta_{ee}$ are the corresponding oscillation parameters, L is the neutrino flight length and E is the neutrino energy. There are almost no oscillation effects that happen for reactor neutrino energies for 10^{-3} eV^2 or 10^{-5} eV^2 scale at short baselines. On the other hand, the oscillation lengths are quite short for 1 eV^2 scale, of the order of meters.

In practice, the neutrino energy E and its flight length L are distributions with uncertainty, because the experiment suffers from energy, position and dimension resolution effects. It is necessary to average the survival probability over the distributions of E and L [25]. The averaged survival probability can be written as follows:

$$\langle P_{\text{sur}} \rangle = 1 - \frac{1}{2} \sin^2 2\theta_{ee} \left[1 - \left\langle \cos \left(\frac{2 \times 1.267 \Delta m^2_{41} L}{E} \right) \right\rangle \right] \tag{2}$$

with

$$\left\langle \cos \left(\frac{2 \times 1.267 \Delta m^2_{41} L}{E} \right) \right\rangle = \int \cos \left(\frac{2 \times 1.267 \Delta m^2_{41} L}{E} \right) \Phi \left(\frac{L}{E} \right) \mathrm{d} \frac{L}{E} , \tag{3}$$

where $\Phi(L/E)$ is the distribution of L/E. For a Gaussian L/E distribution with average $\langle L/E \rangle$ and standard deviation $\sigma_{L/E}$, Eq. (3) can be calculated analytically by

$$\begin{aligned} &\left\langle \cos \left(\frac{2 \times 1.267 \Delta m^2_{41} L}{E} \right) \right\rangle \\ &= \cos \left(2 \times 1.267 \Delta m^2_{41} \left\langle \frac{L}{E} \right\rangle \right) \exp \left[-\frac{1}{2} \left(2 \times 1.267 \Delta m^2_{41} \sigma_{L/E} \right)^2 \right] . \end{aligned} \tag{4}$$

To re-use the resources in the Daya Bay experiment, we briefly demonstrate some experimental parameters here. There are six functionally identical pressurized water reactors, grouped into three pairs, Daya Bay, Ling Ao and Ling Ao-II, each with a maximum of 2.9 GW thermal power. The two

reactors in each pair are at a distance of 88.8 m. The Daya Bay reactors are located more than 1000 m away from Ling Ao and Ling Ao-II. We design the proposed short baseline experiment around the Daya Bay reactors to reduce the interference from other four reactors as much as possible. With typical commercial reactor fuels, the electron antineutrinos are produced mainly from four isotopes: ^{235}U, ^{238}U, ^{239}Pu, and ^{241}Pu. The flux and energy spectrum of the antineutrinos can be predicted from the decays of the nuclear fission products. The cross section we used in this research contains $\mathbf{O(1/M)}$ recoil correction [26]. There are eight ADs having three cylindrical zones, gadolinium doped liquid scintillator (Gd-LS), liquid scintillator (LS) and mineral oil (MO) from the inner outward, in which the Gd-LS is designed to be the target with the diameter of 3 m. Detailed description can be found in Refs. [22, 23].

Different with the currently running Daya Bay experiment, when we move the ADs to somewhere at short baselines, the overburden will decrease, resulting in an increasing of muon and cosmic ray-induced backgrounds. Meanwhile, the backgrounds from the reactors might become significant. The magnitude and the spectrum of the backgrounds will highly depend on where the ADs are. Modeled on the analysis in Ref. [27], we use a spectrum described by $(1/E^2+\text{flat})$ to represent the backgrounds of the accidental events and the fast neutrons. Additionally, we use an inverse beta decay (IBD) spectrum without distortion to approximately represent the backgrounds of the neutrinos from other four reactors and the backgrounds whose distribution is similar to that of the signal.

Since detailed R&D efforts are being researched now, we use here some assumptions based on previous documents: the ratio of the number of neutrino events from Daya Bay reactors to that of $(1/E^2+1)$ shape backgrounds is 1 [27], and to that of the backgrounds with IBD shape is 100 [22, 23]; the detection efficiency is 50% [28–30] instead of 78% in the underground environment [23]. We will transit to the next part using the aforementioned setups, and test the conceptual proposal.

2.2. χ^2 construction

The χ^2 function can be used to test the hypothesis of no oscillation and get the sensitivity. We construct the χ^2 function as follows, like in Refs. [27, 31, 32]:

$$\chi^2 = \sum_{A,i} \frac{\left[M_i^A - T_i^A\left(1+\alpha_{DB}+\alpha_{dB}^A+\alpha_{Db}^i+\sum_r \omega_r^A\alpha_r\right) - B_i^A\left(1+\alpha_b^A\right)\right]^2}{T_i^A + {T_i^A}^2\sigma_{db}^2 + B_i^A}$$
$$+\sum_A\left[\left(\frac{\alpha_{dB}^A}{\sigma_{dB}^A}\right)^2+\left(\frac{\alpha_b^A}{\sigma_b^A}\right)^2\right]+\sum_i\left(\frac{\alpha_{Db}^i}{\sigma_{Db}^i}\right)^2+\sum_r\left(\frac{\alpha_r}{\sigma_r}\right)^2+\left(\frac{\alpha_{DB}}{\sigma_{DB}}\right)^2, \quad (5)$$

where the observed neutrino events are binned in energy E, with 32 bins from 2 to 10 MeV. T_i^A is the expected events number without neutrino oscillation in the i^{th} energy bin for the A^{th} detector. M_i^A represents the measured events number and is replaced by the calculated value with neutrino oscillation in the absence of real data. B_i^A is the events number of the backgrounds. $\{\alpha_{DB}, \alpha_{dB}^A, \alpha_{Db}^i, \alpha_r, \alpha_b^A\}$ denote a set of nuisance parameters, which are used to introduce different sources of systematic uncertainties. Associated bounding uncertainties of these parameters are $\{\sigma_{DB}, \sigma_{dB}^A, \sigma_{Db}^i, \sigma_r, \sigma_b^A\}$, respectively. The notation of the nuisance parameters and the systematic errors are: the first suffix stands for the properties with respect to detectors, while the second one is with respect to different bins; the capital letters mean that the errors are correlated, while the small letters mean uncorrelated.

— α_{DB} is a variable which corresponds to the signal normalization. The absolute reactor antineutrino normalization, the detection efficiency, the exposure time and many other factors can impact it. In this study, we choose σ_{DB} as 5% following Ref. [24].

— α_{dB}^A accounts for the detector related uncorrelated uncertainty, which may be caused by the target mass, H/Gd ratio, life time, trigger, time cuts, energy cuts, *etc.* We take σ_{dB}^A as 0.5%, larger than the value in Refs. [23, 32], since many factors will be changed more or less when we move the ADs to somewhere at short baselines.

— α_{Db}^i represent the uncertainty of the spectrum, and the detector systematics that are not correlated between energy bins [27]. The σ_{Db}^i are around 2% [33].

— α_r correspond to the reactor related uncorrelated uncertainty. Together with ω_r^A, the weight fraction of contribution from the r^{th} reactor to the A^{th} detector, α_rs finally are involved in controling of the normalization of the predicted events number. They may come from the fluctuation of the reactor power and the ageing of the fuels, also may be influenced by the relative positions between the ADs and the reactors. In this study, we set the σ_r as 2% [32].

— Backgrounds are highly dependent on where the ADs are. We give a value $\sigma_b^A = 10\%$ following Ref. [27].

— σ_{db} is the bin-to-bin uncertainty, which is uncorrelated between energy bins and uncorrelated between ADs. It is not well-understood at present, normally assumed to originate from the uncertainties during the background subtraction and the different energy scale. As there is an approximation of Gaussian distribution of L in the study, we give a default value $\sigma_{db} = 1\%$.

The contributions from other correlated uncertainties are not included in this χ^2 function, because for a measurement using multiple detectors, the impact would not be significant. For simplicity, they are ignored in this analysis. The χ^2 function will be minimized with respect to $\sin^2 2\theta_{ee}$, Δm^2_{41} and the nuisance parameters.

3. Discussion

The detector location requires considering various factors, including the oscillation parameters, the statistics, the landform, the overburden, the available space near the reactors and so on. In this study, we will not discuss the landform, the overburden and the available space in detail. Previous global analyses showed that the favored Δm^2_{41} is of the order of 1 eV^2, and give multiple regions which translate into differences in the oscillation lengths [20, 21, 34]. Thus, it is difficult to predict where the maximum or the minimum oscillation will occur. In terms of statistics, the detected number of reactor antineutrinos is proportional to the $1/L^2$, decreasing with the source–detector distance. We build a coordinate system with the middle point of the two reactors as the origin and the line through them as the X axis. Then, the reactors are located at $(\pm 44.4, 0)$ m, as illustrated in figure 1.

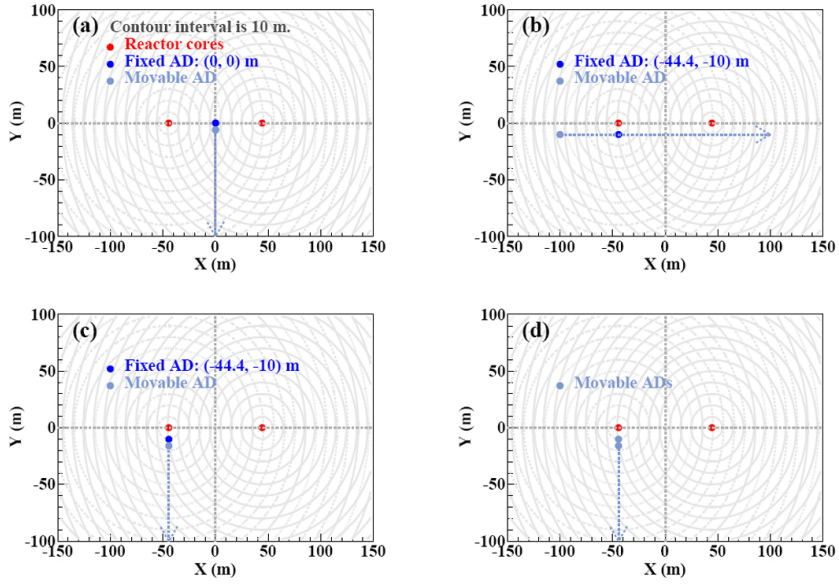


Fig. 1. (Color online) Arrangements of two ADs. (a) consists of a fixed AD at the middle point of the two reactors, and a movable one along the bisector; (b) and (c) consist of a fixed AD at $(-44.4, -10)$ m, and a movable one along the X and Y axis direction, respectively; (d) consists of two ADs which are simultaneously moved away from the reactors, and the distance between the centers of ADs is fixed as 6 m.

The Global Scan method is used to obtain the sensitivity curves [35]. We do not choose other methods since, at present, we focus on the conceptual proposal rather than displaying the most accurate sensitivity curves.

Next, we will discuss the dimension effect and its influence on the sensitivity. Then, we will choose four schemes of two ADs case to illustrate how the arrangement of the detectors would affect the sensitivity. The four schemes are shown in figure 1: (a) consists of a fixed AD at the middle point of the two reactors, and a movable one along the bisector; (b) and (c) consist of a fixed AD at $(-44.4, -10)$ m, and a movable one along the X and Y axis direction, respectively; (d) consists of two ADs which are simultaneously moved away from the reactors, and the distance between the centers of ADs is fixed as 6 m. It is requested that the distance between the centers of two ADs cannot be smaller than 6 m to ensure necessary gap, and the distance between the centers of the AD and the reactor cannot be smaller than 10 m as a result of the realistic situation.

3.1. Dimension effect

The reactors and detectors have dimensions, as listed in Table I. As a result, the neutrino flight length L is a distribution with relatively large uncertainty. Figure 2 shows the distribution of L obtained by Monte Carlo (MC) method, through generating 10^6 pairs of neutrino production positions and detection positions supposing 20 m source–detector distance. Here, we omit the position dependence of the fission rate in the core and assume uniform position distributions. The histogram in black is obtained using the MC method. The thick gray/red curve is a Gaussian fit to the histogram. To further study the influence of source–detector distance on the uncertainty of the neutrino flight length L, we do the same thing for several source–detector distances, and plot the uncertainty of the histograms in figure 3. We can see that the uncertainty of L caused by the dimension effect is about 1 m, and the variation of the uncertainty of L is not much. Actually, the distributions of the neutrino flight length with different source–detector distances look similar but not exactly the same, and using a simple Gaussian function to fit the histogram of L is not accurate.

TABLE I

Geometry size.

Geometry	Radius [m]	Height [m]
Reactor core	1.5	3.6
Detector (Gd-LS)	1.5	3

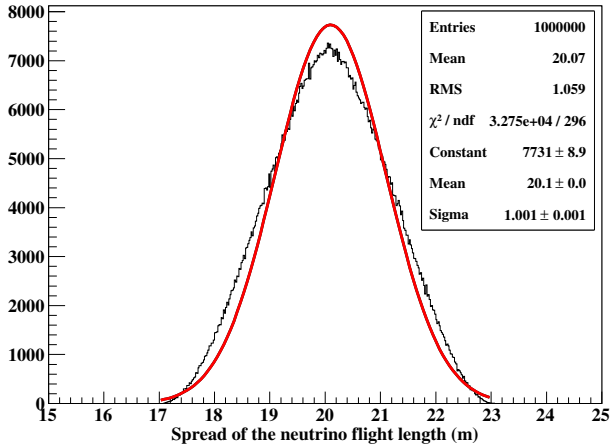


Fig. 2. (Color online) Distribution of the neutrino flight length with 20 m source–detector distance. The histogram in black is obtained by Monte Carlo method. The thick gray/red curve is a Gaussian fit to the histogram.

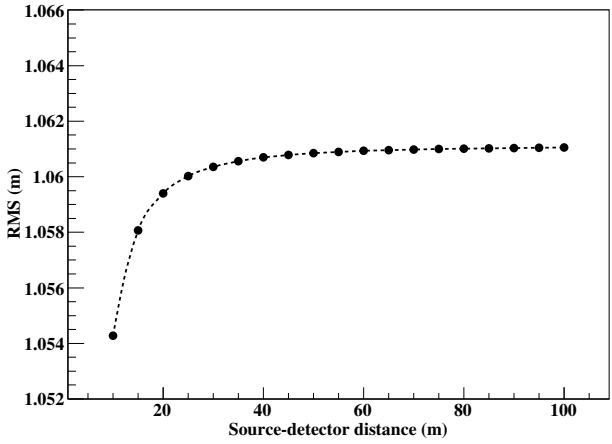


Fig. 3. Variation of the neutrino flight length uncertainty with respect to the source–detector distance.

To take into account the baseline and energy smearing, we average the survival probability over corresponding uncertainties. Since using the MC method to achieve this goal is very time consuming, and obtaining a perfect fitting function of the histogram of L is difficult, we use a Gaussian distribution of L to finish the averaging process analytically [21, 36]. Figure 4 shows the spectrums measured by different methods. Here, we assume that a detector is located 20 m away from a reactor and can measure precise energy and position. The oscillation parameters are assumed as $\sin^2 2\theta_{ee} = 0.1$,

$\Delta m^2_{41} = 1.0$ eV^2. The top canvas contains histograms without and with oscillation, in which the oscillated spectrums are without smearing, and with smearing via averaging the survival probability by MC and analytical method, respectively. To compare the smearing effect, the oscillated histogram without smearing is divided by the two smeared histograms respectively, as shown in the bottom canvas. It can be seen that the influence caused by smearing behaves different among energy bins, and the results from the two methods have a slight difference ($< 0.3\%$). Fully address this discrepancy will make things more complicated. Considering the discrepancy behaves different among energy bins, and different among ADs, which is similar to the bin-to-bin uncertainty, we choose a default value $\sigma_{db} = 1\%$ to partially reflect this discrepancy.

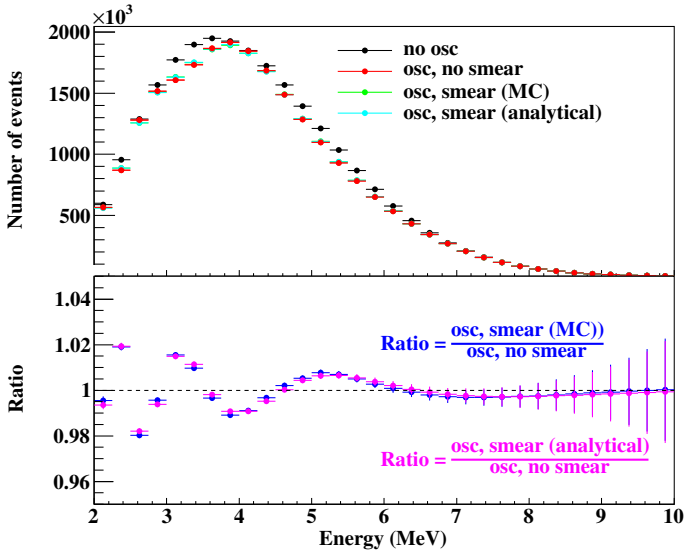


Fig. 4. (Color online) Comparison of the simulated spectrums. The top canvas contains histograms without and with oscillation, in which the oscillated spectrums are without smearing, and with smearing via averaging the survival probability by MC and analytical method, respectively. Here, we assume a detector is located 20 m away from a reactor and can measure precise energy and position. The oscillation parameters are assumed as $\sin^2 2\theta_{ee} = 0.1$, $\Delta m^2_{41} = 1.0$ eV^2.

The smearing can then be treated approximately by analytical method with a much faster speed. As the uncertainties of L and E are independent, we obtain

$$\left(\frac{\sigma_{L/E}}{\langle L/E\rangle}\right)^2 = \left(\frac{\sigma_L}{\langle L\rangle}\right)^2 + \left(\frac{\sigma_E}{\langle E\rangle}\right)^2, \tag{6}$$

where $\langle L \rangle$ and $\langle E \rangle$ are the average distance and energy, σ_L and σ_E are the uncertainties of distance and energy, respectively. Considering that the spatial resolution is around 10 cm [23] and the uncertainty of L due to dimension effect is around 1 m, as shown in figure 3, the σ_L is set to be 1.2 m conservatively. The energy resolution is around $8\%/\sqrt{E}$ [23]. Figure 5 shows the variation of $\sigma_{L/E}$ with respect to the source–detector distance when $E = 1$ MeV, from which we can see that the $\sigma_{L/E}$ decreases with the increase of L, and the contribution of σ_L at very long distances can be ignored.

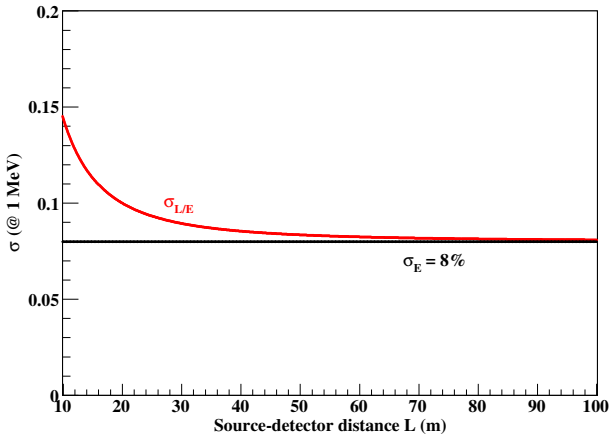


Fig. 5. (Color online) Variation of the $\sigma_{L/E}$ with respect to the source–detector distance when $E = 1$ MeV.

Figure 6 compares the 90% C.L. sensitivity curves supposing two ADs are located at $(-44.4, -10)$ m and $(-44.4, -16)$ m with one year of data taking. It shows that the uncertainty of L plays a significant role in probing large Δm^2_{41} values above 1 eV^2. Because of the big size of the reactor, the room for improvement in the region favored by global fits would be limited, which is consistent with the conclusion in Ref. [37]. That is to say, in order to improve the sensitivity at large Δm^2_{41} region, it is necessary to reduce the σ_L. So when designing the future sterile neutrino experiments, we should strive to choose the sources as small as possible, and use detectors with better spatial resolution. There is a number of proposed experiments that aim to address this, by running on research reactors that are of smaller size, and segmented detectors to improve in-detector resolution.

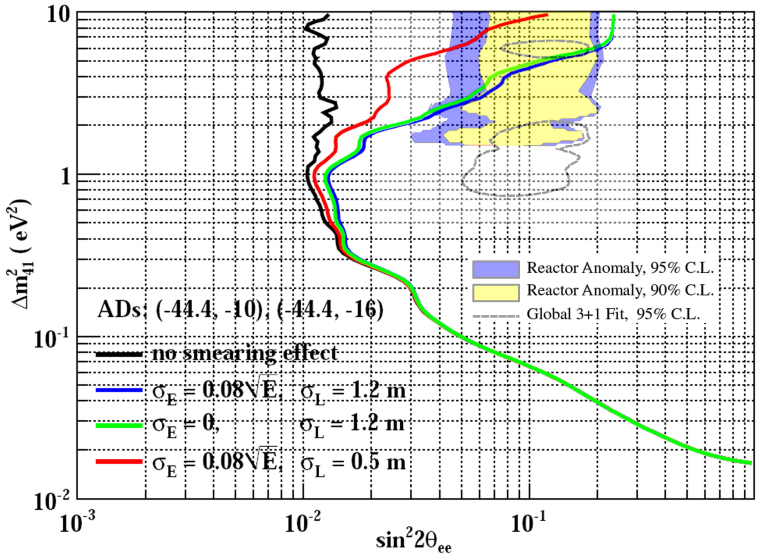


Fig. 6. (Color online) 90% C.L. sensitivity curves with different uncertainties of L and E supposing two ADs are located at $(-44.4, -10)$ m and $(-44.4, -16)$ m with one year of data taking. The dark gray/blue curve reflects a practical case with uncertainties of both L and E. While other two reflect ideal cases, in which the black one assuming we can measure precise L and E without error, and the light gray/green one only involving uncertainty of L. The gray/red curve represents a case assuming the σ_L could be improved to 0.5 m.

3.2. Arrangement of detectors

Multiple experiments looking at different oscillation channels and covering a wide range of L/E regions are required in the future. A multiple-detector approach may provide concrete evidence of spectrum distortion and significantly increase the sensitivity, thus should be adopted [20, 21]. As mentioned before, in this part, we only demonstrate the two ADs case and choose four schemes to illustrate how the arrangement of the detectors would affect the sensitivity.

Using the χ^2 function and Global Scan method described above, in figure 7, we illustrate 90% C.L. sensitivity curves corresponding to the four schemes with one year of data taking, picking out six positions for the movable AD(s) in each subfigure. We can see that better sensitivity can be obtained in the 10^{-2} eV$^2 \lesssim |\Delta m^2_{41}| \lesssim 1$ eV^2 region, but in the region above 1 eV^2, the sensitivity rapidly becomes worse due to the intrinsic deficiency of the commercial reactor size.

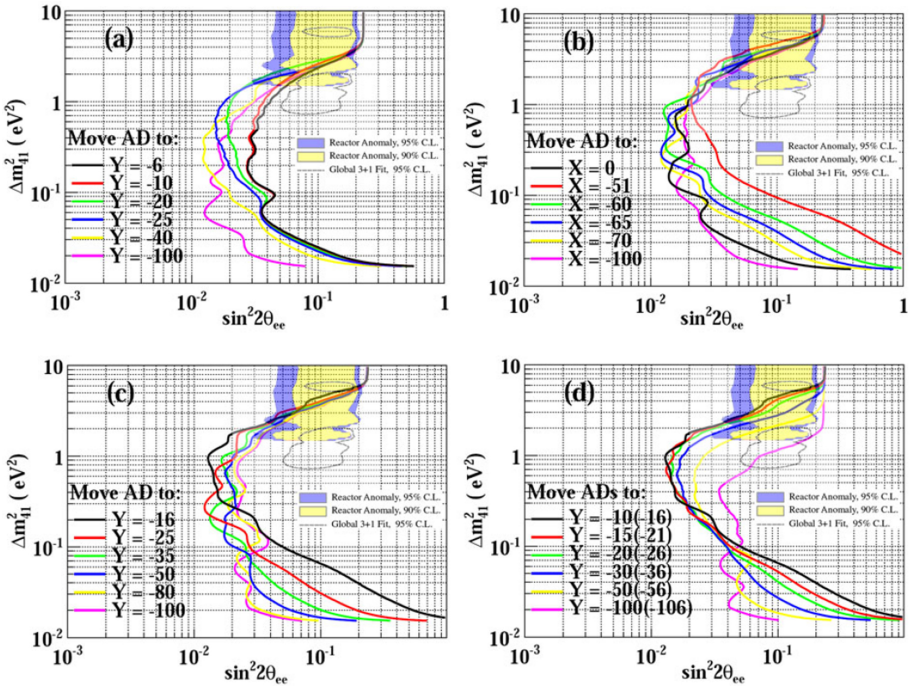


Fig. 7. (Color online) 90% C.L. sensitivity curves corresponding to the four schemes described above with one year of data taking, each scheme picks out six positions for the movable AD(s).

To explicitly demonstrate the variation of the sensitivity with respect to the position changes, we plot the limits on $\sin^2 2\theta_{ee}$ for several Δm^2_{41} in figure 8, and the region of sampled Δm^2_{41} whose limit on $\sin^2 2\theta_{ee}$ is smaller than 0.1 in figure 9. With the position changes of the movable AD(s), the limits on $\sin^2 2\theta_{ee}$ for different Δm^2_{41} seem "oscillated", in which the "valleys" are better position choices for corresponding Δm^2_{41}.

In scheme (a), each detector is positioned equidistant from the two reactors. The advantages would be reflected in the minimum interference from each reactor and simple analysis of the systematic uncertainties. But the AD in the middle of the two reactors is located 44.4 m away from each reactor, farther compared with the distance (10 m between the centers of the fixed AD and the near reactor) in (b) and (c). The longer distance introduces disadvantages due to the averaged survival probability and statistics, leading to a worse sensitivity in the Δm^2_{41} region above 1 eV^2. If one of the AD can be located in the middle of the two reactors, to maximally exclude the parameter space favored by reactor anomaly, the optimized distance between the movable AD and the X axis is around 20 to 25 m. In this range, the sensitivity for various Δm^2_{41} is relatively good except for small Δm^2_{41}. When the

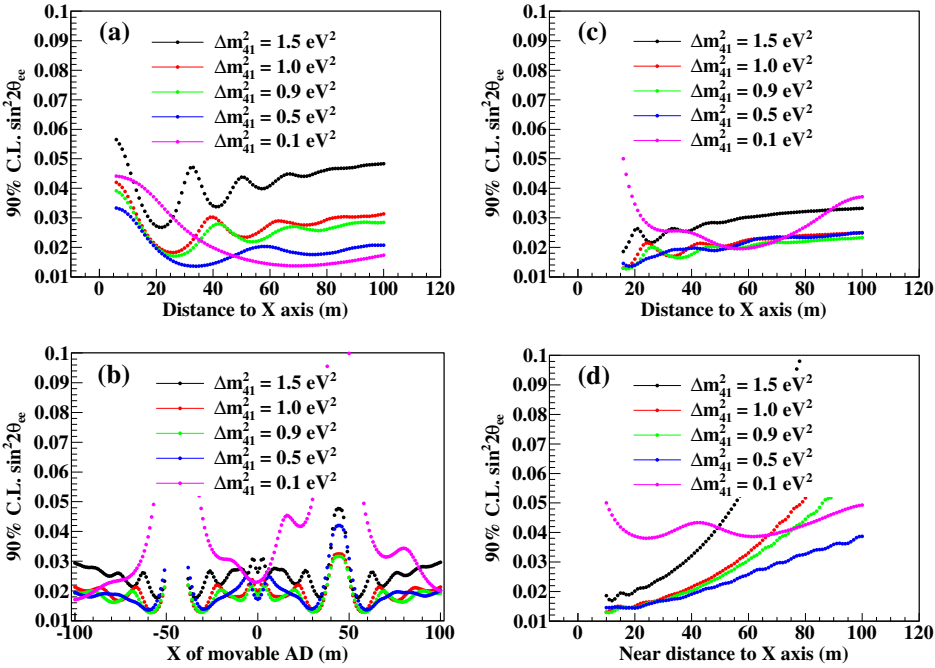


Fig. 8. (Color online) Variation of the limits on $\sin^2 2\theta_{ee}$ for several Δm^2_{41} at 90% C.L. due to the position changes of the movable AD(s).

distance increases to 40 m, the sensitivity becomes better for smaller Δm^2_{41} because the corresponding oscillation length becomes larger, resulting in the possibility to observe more obvious shape distortion.

In scheme (b) and (c), the arrangements of ADs are not symmetrical with the reactors. For Δm^2_{41} with high oscillation frequency, the oscillation will be strongly suppressed at long distances [25], which makes the farther reactor appear as an energy-independent enhancement of the expected rate of events. It can be seen from figure 8 (b) that the sensitivity curves for larger Δm^2_{41} look almost symmetric when the movable AD is located near the reactors. For Δm^2_{41} with low oscillation frequency, theoretically, one of the AD should be located at some position with $(2\times 1.267\Delta m^2_{41}L)/E \sim (2n+1)\pi$ to observe the maximum oscillation effect and the other one should be located at some position with $(2 \times 1.267\Delta m^2_{41}L)/E \sim 2n\pi$, in which n is an integer. To minimize the washing out of the observable oscillation in the detector, the pair of baselines relative to each reactor should be in the similar oscillation period, for example, the middle point of the two reactors. Since Δm^2_{41} is unknown at present, it is hard to decide whether a setup is the most optimized one. As a result, in scheme (b) and (c), taking into account the less suppressed oscillation and higher statistics from the near reactor, the

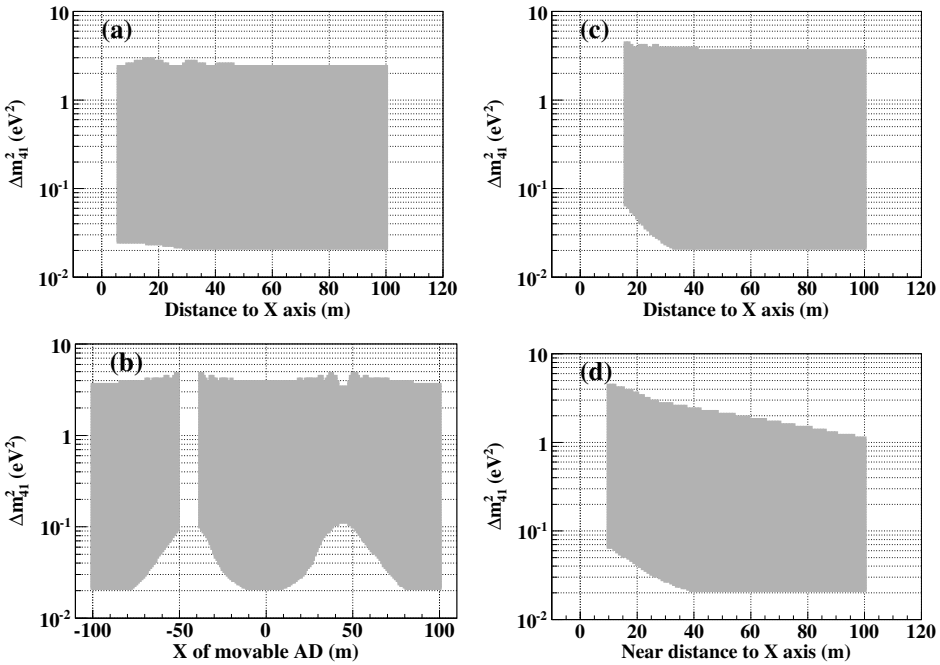


Fig. 9. The Δm^2_{41} region whose limit on $\sin^2 2\theta_{ee}$ at 90% C.L. is smaller than 0.1 with respect to the position changes of the movable AD(s).

sensitivity for Δm^2_{41} around 1 eV^2 performs better than that in scheme (a). The optimized distance between ADs should vary with the true Δm^2_{41} value as well as the relative position between the reactors and detectors. Short distance between ADs, for example 6–10 m, is a good choice to probe large Δm^2_{41} around 1 eV^2.

In scheme (d), the overall sensitivity becomes worse with the increase of the distance between the near AD and the reactors due to the more suppressed oscillation and smaller statistics. For larger Δm^2_{41}, the oscillation is completely suppressed at shorter baseline, which makes the corresponding limit of $\sin^2 2\theta_{ee}$ get worse very quickly. For Δm^2_{41} with long oscillation length, the sensitivity is not good because the two ADs are located at almost the same portion of the total oscillation period. To obtain better sensitivity for Δm^2_{41} around 1 eV^2, the distance between the near AD and the near reactor should be less than 30 m, otherwise the sensitivity would be lost rapidly.

In short, the value of Δm^2_{41} is fixed by nature. By choosing appropriate values of the ratio L/E, different experimental designs can be sensitive to different values of Δm^2_{41}. In our case, if we aim to probe large values of Δm^2_{41} around 1 eV^2, the detectors should be located as close to one of the reactors

as possible. The near reactor will supply higher statistics and less suppressed oscillation, which makes it possible to observe spectrum distortion, while the far reactor will contribute as an energy-independent enhancement of the expected rate of events. The distance between the near AD and the near reactor should be less than 30 m, otherwise the sensitivity would be lost rapidly. The distance between two ADs should be a small value since the oscillation length is of the order of meters. However, considering the big size of the reactor, the exclusion ability of the asymmetric arrangement would be heavily diminished. Thus, if we are not only aiming to probe $\Delta m^2_{41} \sim 1$ eV^2, more flexible choices of detector arrangements can be considered. For Δm^2_{41} with oscillation length of the order of tens of meters, the oscillation amplitude will not be completely suppressed within 100 m. Thus, we should choose some position covering similar portion of the oscillation period from the two reactors to obtain a minimum interference. Since Δm^2_{41} is unknown, we recommend the symmetrical arrangement to avoid factitious insensitivity to some Δm^2_{41}. Instead, we propose to make the multiple detectors cover different fractions of the oscillation periods, the optimized distance between detectors are different for various Δm^2_{41}. If possible, using more detectors, or moving them in a super-huge water pool will help a lot. From a practical standpoint, the symmetrical arrangement is more likely to be implemented because there are already some facilities near the reactors and this symmetrical setups would make future analysis simpler.

4. Conclusion

We have studied the sensitivity of using multiple reactors and detectors at short baselines to observe sterile neutrino. The χ^2 function has been constructed to obtain the experimental sensitivity. We have discussed the influences from the dimension effect and the arrangement of detectors. It was found that the uncertainty of neutrino flight length plays a significant role in probing large Δm^2_{41} values above 1 eV^2, and the room for improvement in this region is limited because of the big size of the commercial reactor. It was also found that better sensitivity can be obtained in the 10^{-2} eV$^2 \lesssim |\Delta m^2_{41}| \lesssim 1$ eV^2 region. If we aim at probing $\Delta m^2_{41} \sim 1$ eV^2, the distance between the near AD and the near reactor should be less than 30 m and the distance between ADs should be a small value of the order of meters. If we aim at probing $\Delta m^2_{41} \sim$ several $\times 0.1$ eV^2, the symmetrical arrangement is recommended in order to avoid factitious insensitivity to some Δm^2_{41}, and the optimized distance between ADs varies from the true Δm^2_{41} value. If one of the ADs can be located in the middle of the two reactors, to exclude the favored parameter space obtained by the reactor anomaly as much as possible, the optimized distance between the movable AD and the X axis is around 20 to 25 m.

This work was supported by a grant from the Ministry of Science and Technology of China (Grant No. 2013CB834303).

REFERENCES

[1] B. Aharmim *et al.* [SNO Collaboration], *Phys. Rev. C* **81**, 055504 (2010).
[2] P. Adamson *et al.* [MINOS Collaboration], *Phys. Rev. Lett.* **107**, 021801 (2011).
[3] M.H. Ahn *et al.* [K2K Collaboration], *Phys. Rev. D* **74**, 072003 (2006).
[4] K. Abe *et al.* [T2K Collaboration], *Phys. Rev. Lett.* **107**, 041801 (2011).
[5] Y. Abe *et al.* [Double Chooz Collaboration], *Phys. Rev. Lett.* **108**, 131801 (2012).
[6] S. Abe *et al.* [KamLAND Collaboration], *Phys. Rev. Lett.* **100**, 221803 (2008).
[7] Y. Fukuda *et al.* [Super-Kamiokande Collaboration], *Phys. Rev. Lett.* **81**, 1562 (1998).
[8] K. Abe *et al.* [Super-Kamiokande Collaboration], *Phys. Rev. D* **83**, 052010 (2011).
[9] J.K. Ahn *et al.* [RENO Collaboration], *Phys. Rev. Lett.* **108**, 191802 (2012).
[10] C. Athanassopoulos *et al.* [LSND Collaboration], *Phys. Rev. Lett.* **77**, 3082 (1996).
[11] Th.A. Mueller *et al.*, *Phys. Rev. C* **83**, 054615 (2011).
[12] P. Huber, *Phys. Rev. C* **84**, 024617 (2011).
[13] F.V. Feilitzsch, A.A. Hahn, K. Schreckenbach, *Phys. Lett. B* **118**, 162 (1982).
[14] K. Schreckenbach, G. Colvin, W. Gelletly, F.V. Feilitzsch, *Phys. Lett. B* **160**, 325 (1985).
[15] A.A. Hahn *et al.*, *Phys. Lett. B* **218**, 365 (1989).
[16] G. Mention *et al.*, *Phys. Rev. D* **83**, 073006 (2011).
[17] J.N. Abdurashitov *et al.*, *Phys. Rev. C* **73**, 045805 (2006).
[18] C. Giunti *et al.*, *Phys. Rev. D* **86**, 113014 (2012).
[19] J. Hamann *et al.*, *Phys. Rev. Lett.* **105**, 181301 (2010).
[20] K.N. Abazajian *et al.*, `arXiv:1204.5379 [hep-ph]`.
[21] J.M. Conrad *et al.*, *Adv. High. Energy. Phys.* **2013**, 163897 (2013).
[22] F.P. An *et al.* [Daya Bay Collaboration], *Phys. Rev. Lett.* **108**, 171803 (2012).
[23] F.P. An *et al.* [Daya Bay Collaboration], *Chin. Phys. C* **37**, 011001 (2013).
[24] F.P. An *et al.* [Daya Bay Collaboration], *Phys. Rev. Lett.* **113**, 141802 (2014).
[25] C. Giunti, C.W. Kim, *Fundamentals of Neutrino Physics and Astrophysics*, Oxford University Press, 2007.

[26] P. Vogel, J.F. Beacom, *Phys. Rev. D* **60**, 053003 (1999).
[27] K.M. Heeger, M.N. Tobin, B.R. Littlejohn, H.P. Mumm, *Phys. Rev. D* **87**, 073008 (2013).
[28] N.S. Bowden *et al.*, *Nucl. Instrum. Methods Phys. Res. A* **572**, 985 (2007).
[29] B. Achkar *et al.*, *Nucl. Phys. B* **434**, 503 (1995).
[30] A.A. Kuvshinnikov *et al.*, *JETP Lett.* **54**, 253 (1991).
[31] H. Sugiyama, O. Yasuda, *Int. J. Mod. Phys. A* **22**, 3407 (2007).
[32] Daya Bay Collaboration, Daya Bay Project Technical Design Report, 2008.
[33] P. Huber, *Phys. Rev. C* **84**, 024617 (2011).
[34] C. Giunti, M. Laveder, *Phys. Rev. D* **84**, 093006 (2011).
[35] G.J. Feldman, R.D. Cousins, *Phys. Rev. D* **57**, 3873 (1998).
[36] R. Gandhi *et al.*, *Phys. Rev. D* **76**, 073012 (2007).
[37] O. Yasuda, *Acta. Phys. Pol. B* **42**, 2379 (2011).